Available online at www.sciencedirect.com
SCIENCE DIRECT®
Journal of Nuclear Materials 351 (2006) 295–302
journal of nuclear materials
www.elsevier.com/locate/jnucmat

Microstructural analysis of deformation in neutron-irradiated fcc materials

N. Hashimoto *, T.S. Byun, K. Farrell

Metals and Ceramics Division, Oak Ridge National Laboratory, 1 Bethel Valley Rd., P.O. Box 2008, BLDG 4500S, Oak Ridge, TN 37831-6136, USA

Abstract

Plastically deformed microstructures in neutron-irradiated face centered cubic (fcc) materials, copper, nickel, and 316 stainless steel (316SS), were investigated by transmission electron microscopy (TEM). Neutron irradiation in the range of 65–100 °C up to 1 displacement per atom (dpa) induced a high number density of black spots, stacking fault tetrahedra (SFT) and Frank loops, which resulted in irradiation-induced hardening. Deformation of irradiated fcc materials induced various microstructures, such as dislocation channels, stacking faults, and twins. In the 316SS irradiated to 0.1–0.8 dpa, the deformation microstructure consisted of a mixture of dislocation bands, tangles, twins, dislocation channels, and also martensite phase. Deformation-induced martensite transformation tends to occur with dislocation channeling, suggesting that localized deformation could lead to transformation of austenite to martensite at a high stress level. At higher irradiation doses (0.1–1 dpa), dislocation channeling became the dominant deformation mode in fcc materials, and is coincident with prompt plastic instability at yield. The channel width seems to be wider when the angle between tensile direction and dislocation slip direction is close to 45°. Furthermore, the correlation between channel width and resolved shear stress appears to be material dependent, with copper having the greatest slope and 316SS the smallest.

1. Introduction

Irradiation-induced hardening in materials is typically accompanied by a severe decrease in uniform plastic elongation. The decrease in tensile ductility associated with low temperature neutron irradiation often leads to the loss of strain hardening capacity, especially at higher doses (>0.1 dpa) [1–7]. These mechanical property changes observed following low temperature irradiation are usually due to the presence of irradiation-induced defect clusters such as black dots, faulted dislocation loops (Frank loop), and stacking fault tetrahedra (SFT), that act as obstacles to dislocation motion during deformation. A general tendency has been observed in many irradiated materials for the radiation-induced defect structure to promote inhomogeneous deformation: dislocation channeling, twinning, and martensite formation, especially in low stacking fault energy materials such as austenitic stainless steels [8–10].

In the channeling process, the mobile dislocations cut, annihilate, and/or combine with the defect clusters on the slip plane during glide. Subsequent

* Corresponding author. Tel.: +1 865 576 2714; fax: +1 865 574 0641.
E-mail address: hashimoton@ornl.gov (N. Hashimoto).

0022-3115/$ - see front matter © 2006 Elsevier B.V. All rights reserved.
doi:10.1016/j.jnucmat.2006.02.032

dislocations will tend to glide more easily along this same path, cleaning out additional defect clusters resulting in a channel free of defects. The increased slip band spacing that results from dislocation channeling reduces macroscopic displacement over a fixed dimension and hence reduces bulk ductility. Dislocation channel deformation has been seen in wide variety of materials [11,12], but the understanding of radiation-induced hardening effects on deformation is limited. Therefore, it is important to clarify the relationship between irradiation-induced defect clusters and dislocation channel deformation in neutron-irradiated materials.

The present paper is focused on microstructural evolution of irradiation-induced defect clusters and deformation-induced microstructure in neutron-irradiated fcc materials: copper, nickel, and 316 stainless steel, in order to understand the deformation mechanisms of materials showing loss of strain hardening capacity.

2. Experimental procedure

High-purity polycrystalline nickel and copper and commercial-purity 316 stainless steel (316SS) were used in this study. The chemical compositions and annealing conditions are shown in Table 1. Custom-designed sheet tensile specimens with a gauge section of 8.0 mm long, 1.5 mm wide, and 0.25 mm thick and an overall length of 17.0 mm were irradiated in the range of 65–100 °C in the Hydraulic Tube facility of the High Flux Isotope Reactor (HFIR). This facility permits small aluminum capsules to be shuttled in and out of the reactor core on demand in a stream of coolant water while the reactor is at power. The irradiation exposures ranged from 1.1×10^{21} to 6.3×10^{24} n m^{-2}, $E > 0.1$ MeV, corresponding to nominal atomic displacement levels of 0.0001 dpa to 0.92 dpa. All tensile tests were conducted at room temperature at a crosshead speed of 0.008 mm s^{-1}, corresponding to an initial specimen strain rate of 10^{-3} s^{-1}. The 0.2% offset yield strength (YS), ultimate tensile strength (UTS), uniform elongation (UE), and total elongation (TE) were calculated from the engineering load–elongation curves. Rectangular pieces were cut from the uniform gauge sections of the tensile-tested (broken) specimens for examination by TEM. Electron microscopy observation was performed at Oak Ridge National Laboratory (ORNL) with a JEM-2000FX and a Philips-CM30 transmission electron microscope operating at 200 kV and 300 kV, respectively.

3. Results and discussion

3.1. Irradiation-induced hardening by defect clusters

Fig. 1 shows the tensile properties of the materials irradiated up to 1 dpa. The YS and the UTS of each material increased with increasing irradiation dose. In all the materials, there was no yield point drop in the unirradiated specimen and in specimens irradiated to the lower doses (<0.01 dpa). A yield drop appeared at a 0.01 dpa and increased in size with increasing dose. In nickel, the relative change in YS increased more rapidly at higher doses than in copper and 316SS. The UE and the TE of copper and nickel decreased rapidly at higher doses.

Typical microstructures of the materials after neutron irradiation are shown in Fig. 2. Neutron irradiation at low temperature produced a high number density ($\sim 10^{23}$ m^{-3}) of very small defect clusters ($\sim$3 nm) in all the materials. In low stacking fault energy (SFE) copper, approximately 90% of irradiation-induced defects are stacking fault tetrahedra (SFT), and the average SFT size remains constant at about 2.6 nm at higher doses. The rest of defect clusters (10%) in copper were black dots, and were too small to determine their morphology or crystallography from the images. The neutron-

Table 1
Chemical compositions and annealing conditions of materials used in this study

	Chemical composition	Heat treatment
Cu	99.999% purity 1.6S–0.09Cr–0.22Ni–0.1 P–0.27Fe–4.8Ag (ppm)	Annealed at 450 °C for 30 min
Ni	99.99% purity	Annealed at 900 °C for 30 min
316SS	Fe–17.15Cr–13.45Ni–2.34Mo–0.1 Cu–1.86Mn–0.059C–0.57Si–0.018 S–0.024P–0.02Co–0.031N (wt%)	Annealed at 1050 °C for 30 min

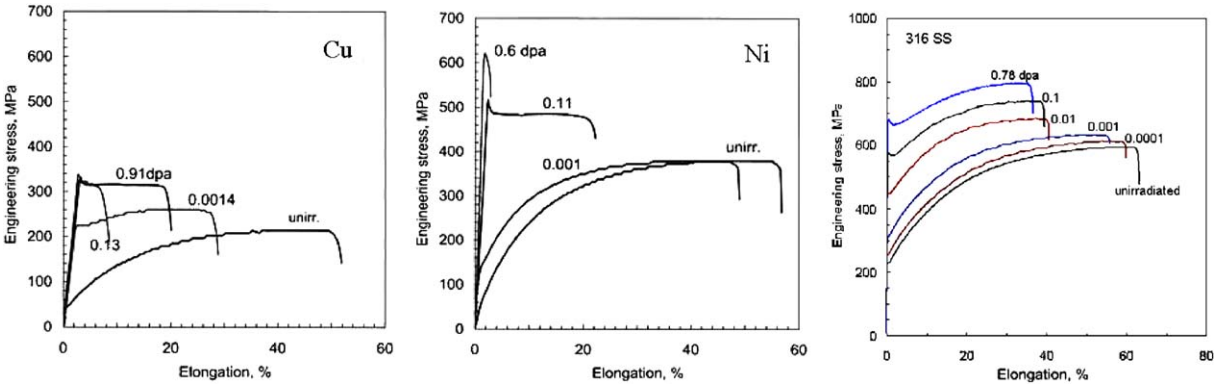

Fig. 1. Room temperature tensile properties of the materials irradiated up to 1 dpa.

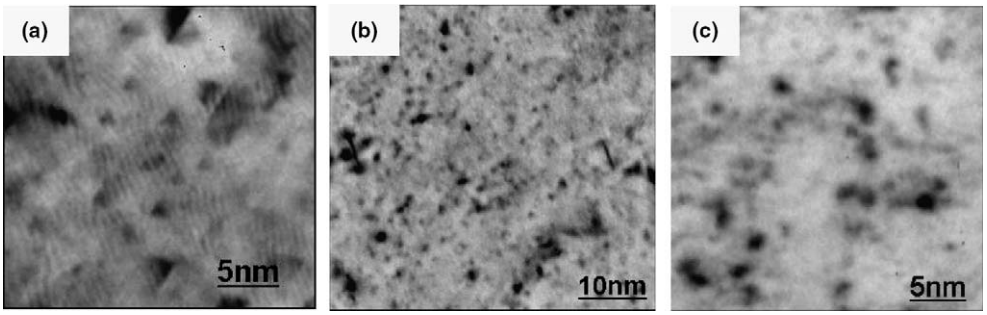

Fig. 2. Microstructures of (a) Cu, (b) Ni, and (c) 316SS irradiated to 0.1 dpa.

irradiated nickel, which has medium SFE, included a high number density of small SFT (approximately 60% of the total defect density) and a low number density of black dots and faulted loops on {1 1 1} planes (Frank loops). In the case of neutron-irradiated 316SS, there were no SFT observed but a high number density of black dots and Frank loops were observed at the highest dose (1 dpa). Measured defect cluster parameters are listed in Table 2, and the number density of defect clusters in each material was plotted as a function of dose in Fig. 3. Total cluster density in each material increases with increasing dose and reaches a saturation level at 0.1 dpa.

From simple geometric considerations of a dislocation traversing a slip plane which intersects randomly distributed obstacles of diameter d and atomic density N, the increase in the uniaxial tensile

Table 2
Summary of observed defect clusters in neutron-irradiated FCC materials

	Dose (dpa)	SFT		Frank loop		Black dot	
		Number density (m^{-3})	Mean size (nm)	Number density (m^{-3})	Mean size (nm)	Number density (m^{-3})	Mean size (nm)
Cu	0.013	1.9×10^{23}	1.6	–	–	$<1\times10^{23}$	1.0
	0.13	6.7×10^{23}	2.5	–	–	$<1\times10^{23}$	1.0
	0.92	7.0×10^{23}	2.6	–	–	$<1\times10^{23}$	1.0
Ni	0.11	3.5×10^{23}	1.0	$<1\times10^{23}$	12.5	$<1\times10^{23}$	1.0
	0.6	6.0×10^{23}	2.0	$<1\times10^{23}$	7.5	$<1\times10^{23}$	1.0
316SS	0.01	–	–	–	–	8.0×10^{22}	1.5
	0.15	–	–	–	–	2.5×10^{23}	1.6
	0.79	–	–	1×10^{23}	3.5	3.0×10^{23}	1.8

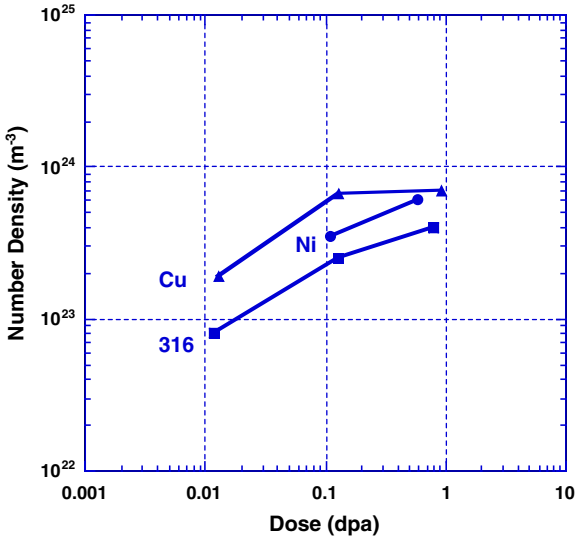

Fig. 3. Number density of defect clusters in materials as a function of irradiation dose (Cu: SFT + black dot, Ni: SFT + Frank loop + black dot, 316SS: Frank loop + black dot).

stress for polycrystalline specimens ($\Delta\sigma$) in a material is given by the well-known dispersed barrier hardening equation [1,2,13], $\Delta\sigma = M\alpha\mu b(Nd)^{1/2}$, where μ is the shear modulus, b is the magnitude of the Burgers vector of the glide dislocation ($a_0/\sqrt{2}$ for FCC, where a_0 is the lattice parameter), M is the Taylor factor (3.06), and α is average barrier strength of the radiation-induced defect clusters. Based on this equation and the measurements carried out in this experiment, a value of $\alpha \approx 0.20$ was obtained for SFT in copper. Recent experimental estimates range from $\alpha \approx 0.10$–0.25 for copper [14,15] and austenitic stainless steel [2,8,16] irradiated at low temperatures. In this study, neutron-irradiated nickel and 316SS exhibited mixture of defect clusters, so that the barrier strength for different type of cluster could not be estimated. Instead, the average barrier strength for clusters in nickel and 316SS was estimated to be 0.4–0.6. This greater barrier strength than that in copper is probably due to the existence of Frank loops in neutron-irradiated nickel and 316SS. The estimated α value of a Frank loop has been reported to be 0.5 for neutron-irradiated 316LN irradiated at low temperatures [17].

3.2. Deformation-induced microstructure in neutron-irradiated FCC materials

Fig. 4 shows the general deformation microstructure at low magnification for the three materials after irradiation up to 0.9 dpa. Dislocation channeling is visible as narrow bands, which have been largely cleaned of the fine defect structure. Dislocation channeling can be practically distinguished from twinning: streaks arising from twin boundary should be found in the diffraction pattern because twin is a very thin platelet. In general, dislocation channeling begins to occur above a critical dose/hardening level (corresponding to a cluster density of $N > \sim 1 \times 10^{23}/\mathrm{m}^3$ for copper tested at room temperature [2,14]). In this study, the deformed fcc materials, copper, nickel, and 316SS, exhibited channels only at doses higher than 0.1 dpa. Dislocation channels tend to be present on {1 1 1} glide planes in copper and nickel, and on {1 1 1} and {1 0 0} glide planes in 316SS. Channel width in 316SS appears to be narrower than that in copper and nickel. Dislocation channeling in copper and nickel is coincident with prompt plastic instability at yield, suggesting that the loss of work hardening capacity in irradiated copper and nickel at higher doses is mainly due to dislocation channeling in local regions that experience a high resolved shear stress.

In 316SS irradiated to 0.1–0.8 dpa, the deformation microstructure consisted of a mixture of dislo-

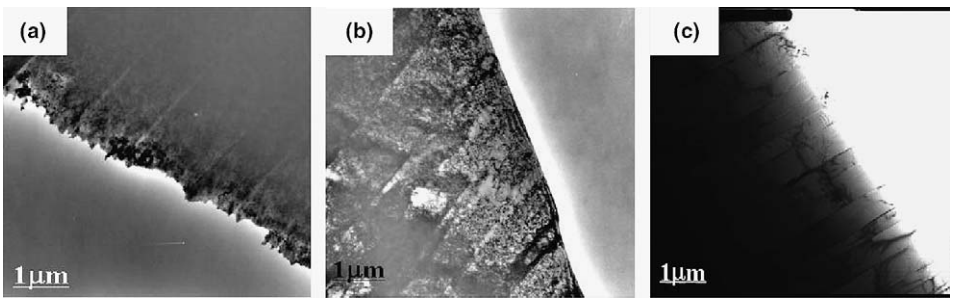

Fig. 4. General microstructure of dislocation channel deformation in (a) Cu, (b) Ni, and (c) 316SS irradiated to 0.92, 0.6, and 0.79 dpa, respectively. Dislocation channels are present on {1 1 1} in Cu and Ni, and on {1 1 1} and {1 0 0} in 316SS.

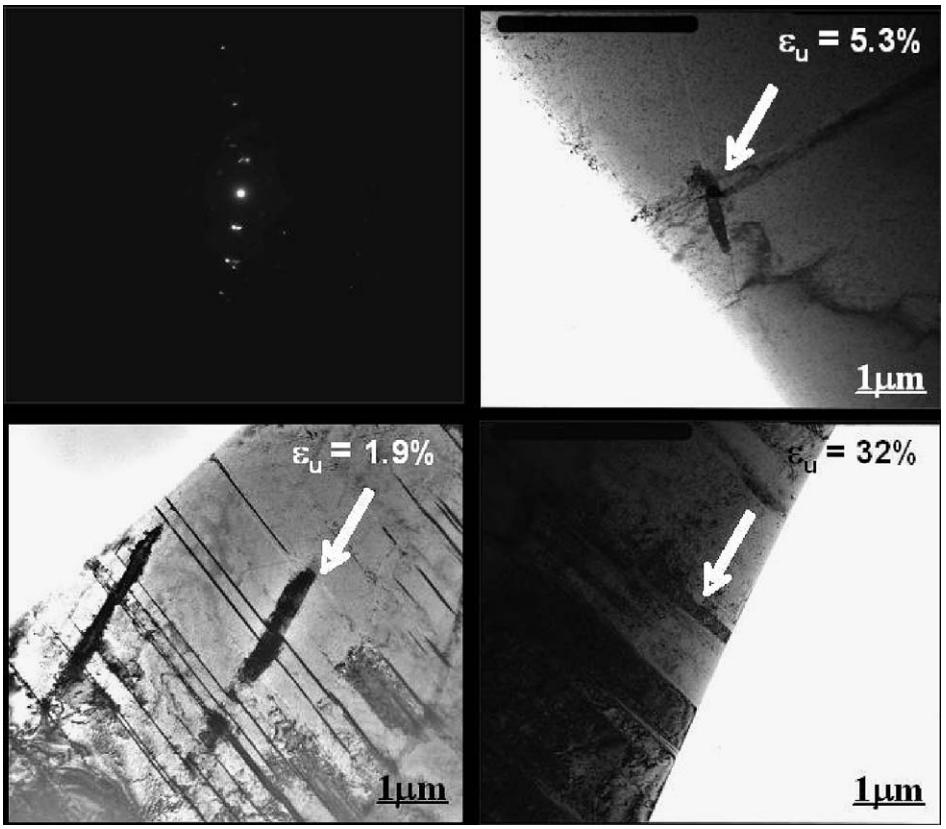

Fig. 5. Microstructure of deformed 316SS irradiated to 1 dpa. Deformation-induced martensite transformation (arrowed region) was observed along with dislocation channeling at each strain level.

cation bands, tangles, twins, dislocation channels, and also martensite phase. Fig. 5 shows the microstructure of deformed 316SS irradiated to 1 dpa. Deformation-induced martensite phase running with dislocation channels in {1 1 1} planes were observed at each strain level, suggesting that localized deformation could lead to martensite transformation at a high stress level.

3.3. Effect of orientation on dislocation channeling

When a tensile specimen is loaded in uniaxial tension, the applied stress, σ_{as}, is resolved on the slip planes in the material. The resolved shear stress, τ_{rss}, on any given plane is determined by the angles between the plane normal and the applied stress (ϕ) and between the slip direction and the applied stress (θ) : $\tau_{rss} = \sigma_{as}\cos(\phi)\cos(\theta)$. The relationship between τ_{rss} and σ_{as} is complicated by the fact that maximum resolved shear stress will vary from one grain to another. In addition, material compatibility and continuity act to limit the deformation of any one grain that may be favorably oriented by slip. In this study, rectangular shaped TEM samples (1.5×2.0 mm) were taken from the uniform strain region of the tensile-tested (broken) specimens in order to monitor the tensile axis orientation of the deformed gauge region in the TEM. With the long edge of the rectangular specimen set parallel to the TEM holder, the deformation channel orientation with respect to the tensile direction within the grain could be determined by the diffraction pattern. On the assumption that all the grains in the material deformed uniformly and grain rotation during deformation is negligible, the resolved shear stress for each dislocation channel observed was estimated using the value of the UTS.

Fig. 6 shows the dependence of the resolved shear stress on the angle between the tensile axis and either the slip plane normal or slip direction in each grain where channeling was measured. Since the maximum resolved shear stress varies from one grain to another when the tensile specimen is loaded in uniaxial tension, the values of estimated resolved

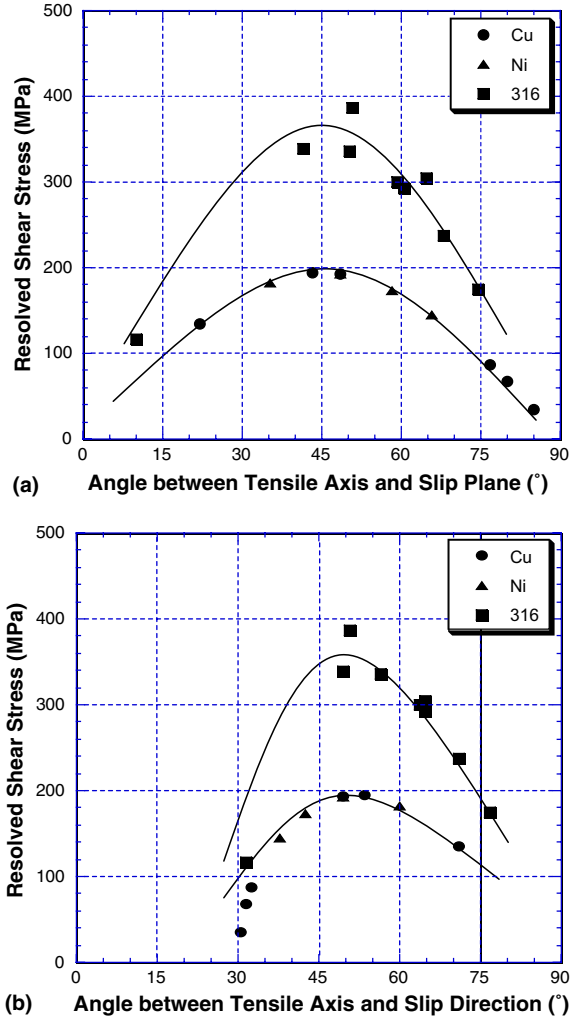

Fig. 6. Dependence of resolve shear stress on the angle between tensile axis and slip plane normal (a) and slip direction (b) in grain where channeling occurred.

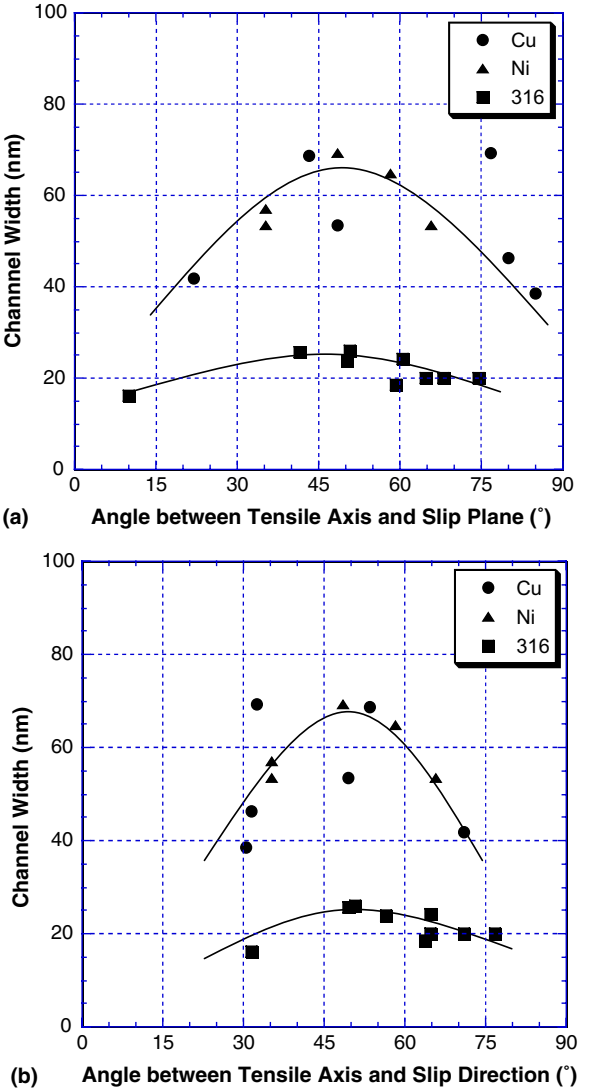

Fig. 7. Dependence of channel width on the angle between tensile axis and slip plane normal (a) and slip direction (b).

stress varied widely for different dislocation channels. However, in all the materials, there is a tendency for the resolved shear stress to be the greatest when the angle is around 45° due to simple geometrical considerations. The Schmid factor, m, is defined as the ratio of the resolved shear stress to the axial stress, $m = \cos(\phi)\cos(\theta)$. The maximum value of m occurs when the shear plane is at a 45° angle to the applied stress.

Fig. 7 shows the dependence of measured dislocation channel width on the angle between the tensile axis and either the slip plane normal or the slip direction. It should be noted that there is the same tendency as the resolved shear stress for the channel width to be wider when the angle is around 45°. Of potentially greater significance for understanding the deformation mechanisms in dislocation channeling, the channel width increased with increasing resolved shear stress as seen in Fig. 8. This indicates that the largest localized deformation tends to occur at the highest resolved shear stress level and that there maybe a stress-dependent mechanism that limits the width of the dislocation channel evolution during deformation. Furthermore, there appears to be a material dependence on the correlation between channel width and resolved shear stress; copper exhibited the greatest dependence of channel width on resolved shear stress and 316SS the smallest

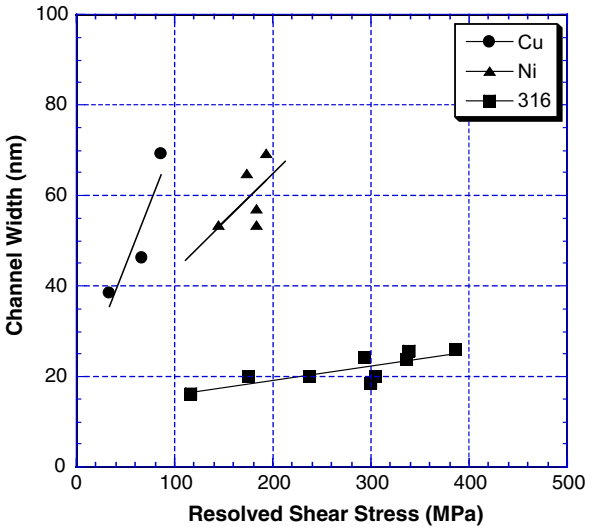

Fig. 8. Relationship between channel width and the resolved shear stress.

(316SS < Ni < Cu). Possible factors controlling this correlation could be the difference of SFE and/or the shear modulus between the materials. However, neither the magnitude of the SFE nor the shear modulus explains the correlation: (316SS: ~20 mJ/m^2 < Cu: ~80 mJ/m^2 < Ni: ~130 mJ/m^2) for SFE and (Cu: 45 100 MPa < 316SS: 56 000 MPa < Ni: 76 500 MPa) for the shear modulus. Assuming that the width of channels reflects 'shearablity' of irradiation-induced defect clusters by moving dislocations, the barrier strength of each cluster could be a key factor for this issue. As discussed above, neutron irradiation at low temperature induced three kinds of defect clusters in the materials: black dots, SFTs, and Frank loops. The existence of Frank loops, which appear to have relatively higher barrier strength [17], increased the average barrier strength in nickel and 316SS. Since the number density of Frank loops in 316SS is greater than in nickel, it is suggested that the material with the most shearable defects could be copper and the least shearable could be 316SS among the materials used in this study. This hierarchy might be able to explain the material dependence on the correlation between channel width and resolved shear stress.

4. Conclusions

The deformation microstructure of irradiated FCC materials copper, nickel, and 316 stainless steel has been investigated by transmission electron microscopy in order to understand the deformation mechanisms of materials showing a loss of strain hardening capacity.

Irradiation-induced defect clusters, consisting predominantly of SFTs in copper, SFTs and Frank loops in nickel, and Frank loops in 316SS were observed at the higher irradiation doses. The estimated barrier strength for defect clusters in the materials was in good agreement with previously reported values. Dislocation channeling occurred in all the deformed materials, and is coincident with prompt plastic instability at yield. Channel width seems to be wider when the angle between tensile direction and dislocation slip direction is close to 45°, corresponding to the maximum resolved shear stress condition. Furthermore, there is a material dependence on the correlation between channel width and resolved shear stress, copper exhibited the greatest dependence and 316SS the smallest.

Acknowledgement

This research was sponsored by the Office of Fusion Energy Sciences, US Department of Energy, under contract No DE-AC05-00OR22725 with UT-Battelle, LLC.

References

[1] U.F. Kocks, Mater. Sci. Eng. 27 (1977) 291.
[2] S.J. Zinkle, Radiat. Eff. Def. Solids 148 (1999) 447.
[3] N. Hashimoto, T.S. Byun, K. Farrell, S.J. Zinkle, J. Nucl. Mater. 336 (2005) 225.
[4] H. Matsui, O. Yoshinari, K. Abe, J. Nucl. Mater. 141–143 (1986) 855.
[5] R. Bajaj, M.S. Wechsler, in: M.T. Robinson, F.W. Young, Jr. (Eds.), Fundamental Aspects of Radiation Damage in Metals, vol. ll, CONF-751006-P2, National Tech. Inform. Service, Springfield, VA, 1975. p. 1010.
[6] N. Hashimoto, T.S. Byun, K. Farrell, S.J. Zinkle, J. Nucl. Mater. 329–333 (2004) 947.
[7] T.S. Byun, K. Farrell, N. Hashimoto, J. Nucl. Mater. 329–333 (2004) 998.
[8] N. Hashimoto, S.J. Zinkle, A.F. Rowcliffe, J.P. Robertson, S. Jitsukawa, J. Nucl. Mater. 283–287 (2000) 528.
[9] J.I. Cole, S.M. Bruemmer, J. Nucl. Mater. 225 (1995) 53.
[10] J.L. Brimhall, J.I. Cole, S.M. Bruemmer, Scripta Metall. Mater. 30 (1994) 1473.
[11] M.S. Wechsler, in: R.E. Reed-Hill (Ed.), The Inhomogeneity of Plastic Deformation, ASM, 1973, p. 19 (Chapter 2).
[12] A. Luft, Prog. Mater. Sci. 35 (1991) 97.
[13] A.K. Seeger, in: Second UN Conference on Peaceful Uses of Atomic Energy, vol. 6, United Nations, New York, 1958, p. 250.
[14] S. Kojima, S.J. Zinkle, H.L. Heinisch, J. Nucl. Mater. 179–181 (1991) 982.

[15] Y. Dai, M. Victoria, in: Microstructure Evolution During Irradiation, in: I.M. Robertson et al. (Eds.), MRS Symposium Proceeding, vol. 439, Materials Research Society, Pittsburgh, 1997, p. 319.
[16] S.J. Zinkle, R.L. Sindelar, J. Nucl. Mater. 155–157 (1988) 1196.
[17] N. Hashimoto, E. Wakai, J.P. Robertson, J. Nucl. Mater. 273 (1999) 95.